

Surface-Tunable Photoluminescence from Block Copolymer-Stabilized Cadmium Sulfide Quantum Dots

C.-W. Wang and M. G. Moffitt*

Department of Chemistry, University of Victoria, P.O. Box 3065,
Victoria, British Columbia, V8W 3V6 Canada

Received June 29, 2004. In Final Form: October 4, 2004

The static and time-resolved photoluminescence properties of polystyrene-*b*-poly(acrylic acid) (PS-*b*-PAA)-stabilized cadmium sulfide quantum dots (CdS QDs) have been characterized for the first time, demonstrating tunable emission spectra and quantum yields via different chemical treatments of the PAA layer. Samples with the PAA layer in its cadmium carboxylate form showed more-intense band-edge emission and relatively high quantum yields compared with samples in which the PAA layer was in its acid form. This activation effect is explained in terms of passivation of trap sites on the QD surface by specific interactions between the QD and the cadmium-neutralized PAA layer. Lifetimes of band-edge and trap state emission for the various samples ranged from 40 to 61 ns and 244 to 360 ns, respectively. Impressive long-term stability was also shown for a sample of cadmium-neutralized PS-*b*-PAA-stabilized QDs dispersed in toluene, which maintained 90% of its photoluminescence over 57 days aging under ambient conditions. It is also shown that Cd²⁺ activation of photoluminescence does not occur when Mg²⁺ ions are added to similar QD solutions, indicating potential of these block copolymer-stabilized QDs as Cd²⁺-selective sensors. Irrespective of chemical treatment of the PAA layer, the external PS brush layer effectively stabilized all samples in various organic solvents, resulting in clear CdS colloids with no observed precipitation over several months. Dynamic light scattering and gel permeation chromatography revealed differences in the aggregation numbers and hydrodynamic radii of colloidal QDs for different treatments of the PAA layer, attributed to the lower solubility of the poly(cadmium acrylate) blocks compared to the PAA blocks in the acid form. Finally, it was demonstrated that the PS-*b*-PAA-stabilized QDs could be well dispersed in PS homopolymer, producing optically transparent photoluminescent films which retained the emission features of the colloidal QDs. Stable and surface-tunable optical properties via the PAA layer and polymer solubility and processability via the PS layer make these PS-*b*-PAA-stabilized CdS QDs exciting “building blocks” for the bottom-up assembly of functional hierarchical materials for photonics, sensors, and bio-labeling applications.

Introduction

Colloidal semiconducting nanoparticles, or quantum dots (QDs), have attracted a great deal of interest in recent years due to their size-dependent optical and electronic properties, which arise from quantum confinement and surface effects.^{1–6} In particular, the intense and size-tunable light emission exhibited by colloidal II/IV semiconductors (e.g., CdS, CdSe) have made these nanoparticles intriguing candidates as fluorescent bio-labels or as functional elements in materials with potential applications in photonics, electroluminescence, and sensing. A key issue behind the synthesis of colloidal QDs is their functionalization with appropriate organic ligands.⁷ This organic surface layer provides the inorganic nanoparticles with solubility, stability, and processability in a range of organic media through favorable interactions with the surrounding environment. As well, specific interactions between the organic layer and the nanoparticle surface can play an important role toward passivating trap states caused by surface defects, thus optimizing photoluminescence quantum yields.^{7–11}

For future applications of colloidal QDs in thin films and three-dimensional device structures, their facile incorporation into various polymer environments will be of critical importance. However, conventional synthetic methodologies for colloidal CdSe and CdS produce tri-*n*-octylphosphine oxide (TOPO)-stabilized nanoparticles that tend to undergo aggregation in common polymers such as polystyrene and poly(methyl methacrylate), resulting in a loss of optical clarity and quenching of photoluminescence.^{9,12} Among the various strategies for obtaining nanocomposites of well-dispersed semiconducting QDs in a polymer matrix,^{12–16} several recent studies have targeted the production of discrete colloidal building blocks with a polymeric layer coating the inorganic nanoparticle.^{17–23} This “building block” concept offers an exciting degree of

* Author to whom correspondence should be addressed. E-mail: mmoffitt@uvic.ca.

(1) Trindade, T.; O'Brien, P.; Pickett, N. L. *Chem. Mater.* **2001**, *13*, 3843.

(2) Murray, C. B.; Kagan, C. R.; Bawendi, M. G. *Annu. Rev. Mater. Sci.* **2000**, *30*, 545.

(3) Alivisatos, A. P. *J. Phys. Chem.* **1996**, *100*, 13226.

(4) Weller, H. *Angew. Chem., Int. Ed. Engl.* **1993**, *32*, 41.

(5) Steigerwald, M. L.; Brus, L. E. *Acc. Chem. Res.* **1990**, *23*, 183.

(6) Henglein, A. *Chem. Rev.* **1989**, *89*, 1861.

(7) Kim, S.; Bawendi, M. G. *J. Am. Chem. Soc.* **2003**, *125*, 14652.

(8) Ni, T.; Nagesha, D. K.; Robles, J.; Materer, N. F.; Mussig, S.; Kotov, N. A. *J. Am. Chem. Soc.* **2002**, *124*, 3980.

(9) Murray, C. B.; Norris, D. J.; Bawendi, M. G. *J. Am. Chem. Soc.* **1993**, *115*, 8706.

(10) Herron, N.; Wang, Y.; Eckert, H. *J. Am. Chem. Soc.* **1990**, *112*, 1322.

(11) Dannhauser, T.; O'Neil, M.; Johansson, K.; Whitten, D.; McLendon, G. *J. Phys. Chem.* **1986**, *90*, 6074.

(12) Lee, J.; Sundar, V. C.; Heine, J. R.; Bawendi, M. G.; Jensen, K. F. *Adv. Mater.* **2000**, *12*, 1102.

(13) Hirai, T.; Watanabe, T.; Komasa, I. *J. Phys. Chem B* **2000**, *104*, 8962.

(14) Pavel, F. M.; Mackay, R. A. *Langmuir* **2000**, *16*, 8568.

(15) Zhang, H.; Cui, Z.; Wang, Y.; Zhang, K.; Ji, X.; Lu, C.; Yang, B.; Gao, M. *Adv. Mater.* **2003**, *15*, 777.

(16) Petruska, M. A.; Bartko, A. P.; Klimov, V. I. *J. Am. Chem. Soc.* **2004**, *126*, 714.

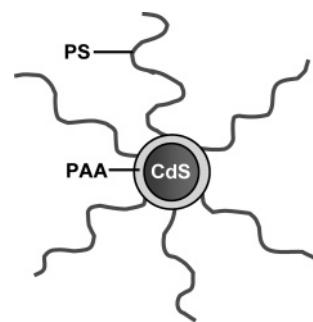
(17) Lemon, B. I.; Crooks, R. M. *J. Am. Chem. Soc.* **2000**, *122*, 12886.

(18) Guo, W.; Li, J. J.; Wang, A.; Peng, X. *J. Am. Chem. Soc.* **2003**, *125*, 3901.

versatility for producing nanocomposite structures since an appropriate polymer layer can solubilize hybrid nanoparticles in a matrix of the equivalent homopolymer²⁴ or mediate the self-assembly of colloidal QDs via steric repulsions between approaching polymer brushes, resulting in ordered nanocomposites.²⁵ Following earlier work by Murphy and co-workers,^{26,27} Lemon et al. reported the synthesis of CdS nanoparticles in a poly(amidomaine) dendrimer nanoreactor, resulting in discrete dendrimer-coated fluorescent nanoparticles.¹⁷ A ligand-exchange approach was used by Guo et al. to encapsulate preformed CdSe/CdS core-shell nanoparticles in cross-linked dendron “boxes”.¹⁸ Poly(caprolactone)-coated CdS nanoparticles have been synthesized by Carrot et al. via covalent surface attachment of thiol-functional polymer chains.¹⁹ Other studies by Emrick and co-workers have effectively demonstrated the surface functionalization of TOPO-covered CdSe QDs with polystyrene, polyolefin, and poly(ethylene glycol) using ligand-exchange and surface polymerization strategies.^{20–22} Recently, Potapova et al. have applied electrostatic binding of poly(acrylamide) ionomers to negatively charged CdSe/ZnS colloidal QDs to the production of hybrid polymer–inorganic nanoparticles.²³

An alternative and relatively direct route to polymer-coated semiconductor colloids utilizes templates of microphase-separated block copolymers.^{25,28–40} This approach has been applied in a number of studies in which amphiphilic block copolymers undergo self-assembly to form nanoscale domains of metal ion-containing or metal ion-complexing blocks in the solid-state^{28,29,33} or block copolymer micelles in organic solvents with insoluble cores of the metal ion-containing blocks.^{25,30–32,34–40} The metal ions are then chemically transformed via simple reduction or precipitation reactions into metal or semiconducting nanoparticles. Under certain conditions, single nanoparticles can be grown inside each spherical core or microdomain, providing the advantage of thermodynamic

Scheme 1



nanoparticle size control via the aggregation number or the degree of metal ion loading.^{30–32} In some cases, the block copolymer template can play the role of a stabilizer following nanoparticle synthesis, yielding colloidal inorganic nanoparticles coated by two covalently linked polymer layers: an inner layer of insoluble blocks and an outer “brush” layer of soluble blocks.

Moffitt et al. demonstrated that single CdS QDs could be synthesized in the ionic cores of polystyrene-*b*-poly(cadmium acrylate) (PS-*b*-PACd) by exposing the block ionomer to H₂S in the solid state; the resulting block copolymer micelles could then be dispersed in organic solvents to obtain stable and optically clear colloids consisting of QDs stabilized by polystyrene-*b*-poly(acrylic acid) (PS-*b*-PAA) (Scheme 1).³⁰ The stability of the micelles to repeated precipitation into methanol was found to increase with reneutralization of the PAA layer with NaOH or cadmium acetate dihydrate. However, the photoluminescence properties and solution structure of the polymer-coated QDs were not explored.

One intriguing aspect of these PS-*b*-PAA-stabilized colloidal QDs is the chemical reactivity of the carboxylic acid groups in the PAA layer surrounding the nanoparticle surface. It has been shown that reloading the carboxylic acid groups with metal ions and subsequent chemistry can be used to increase the nanoparticle size or, in principle, to obtain inorganic core-shell particles.^{30,33} Here, we demonstrate that simple chemistry within the PAA layer can be used to tune the photoluminescence of the QDs, allowing for optimization of quantum yields, as well as light emission that can be “switched” as a function of the chemical form of PAA. The observed tunable photoluminescence is attributed to changes in the surface environment of the CdS nanoparticles, which result in variations in the density and nature of surface trap states.^{6–11,41–53} Spanhel et al.⁴¹ showed that the addition of Cd²⁺ ions at high pH dramatically enhances the quantum yields of colloidal CdS QDs; this type of surface

(19) Carrot, G.; Scholz, S. M.; Plummer, C. J. G.; Hilborn, J. G.; Hendrick, J. L. *Chem. Mater.* **1999**, *11*, 3571.

(20) Erskine, L. L.; Emrick, T.; Alivisatos A. P.; Frechet J. M. J. *Abstr. Pap. Am. Chem. Soc.* 219: 387-POLY Part 2, Mar 26, 2000.

(21) Skaff, H.; Ilker, M. F.; Coughlin, E. B.; Emrick, T. *J. Am. Chem. Soc.* **2002**, *124*, 5729.

(22) Skaff, H.; Emrick, T. *Chem. Commun.* **2003**, 52.

(23) Potapova, I.; Mruk, R.; Prehl, S.; Zentel, R.; Basche, T.; Mews, A. *J. Am. Chem. Soc.* **2003**, *125*, 320.

(24) Corbierre, M. K.; Cameron, N. S.; Sutton, M.; Mochrie, S. G. J.; Lurio, L. B.; Ruhm, A.; Lennox, R. B. *J. Am. Chem. Soc.* **2001**, *123*, 10411.

(25) Spatz, J. P.; Herzog, T.; Mössmer, S.; Ziemann, P.; Möller, M. *Adv. Mater.* **1999**, *11*, 149.

(26) Sooklal, K.; Hanus, L. H.; Ploehn, H. J.; Murphy, C. J. *Adv. Mater.* **1998**, *10*, 1083.

(27) Huang, J.; Sooklal, K.; Murphy, C. J.; Ploehn, H. J. *Chem. Mater.* **1999**, *11*, 3595.

(28) Möller, M.; Künstle, H.; Kunz, M. *Synth. Met.* **1991**, *41–43*, 1159.

(29) Cummins, C. C.; Schrock, R. R.; Cohen, R. E. *Chem. Mater.* **1992**, *4*, 27.

(30) Moffitt, M.; McMahon, L.; Pessel, V.; Eisenberg, A. *Chem. Mater.* **1995**, *7*, 1185.

(31) Möller, M.; Spatz, J. P. *Curr. Opin. Colloid Interface Sci.* **1997**, *2*, 177.

(32) Förster, S.; Antonietti, M. *Adv. Mater.* **1998**, *10*, 195.

(33) Cohen, R. E. *Curr. Opin. Solid State Mater. Sci.* **1999**, *4*, 587.

(34) Wang, D.; Cao, Y.; Zhang, X.; Liu, Z.; Qian, X.; Ai, X.; Liu, F.; Wang, D.; Bai, Y.; Li, T.; Tang, X. *Chem. Mater.* **1999**, *11*, 392.

(35) Underhill, R. S.; Liu, G. *Chem. Mater.* **2000**, *12*, 2082.

(36) Qi, L.; Colfen, H.; Antonietti, M. *Nano Lett.* **2001**, *1*, 61.

(37) Zhao, H.; Douglas, E. P.; Harrison, B. S.; Schanze, K. S. *Langmuir* **2001**, *17*, 8428.

(38) Zhao, H.; Douglas, E. P. *Chem. Mater.* **2002**, *14*, 1418.

(39) Yang, C.-S.; Awaschalom, D. D.; Stucky, G. D. *Chem. Mater.* **2002**, *14*, 1277.

(40) Zhang, M.; Drechsler, M.; Müller, A. H. E. *Chem. Mater.* **2004**, *16*, 537.

(41) Spanhel, L.; Haase, M.; Weller, H.; Henglein, A. *J. Am. Chem. Soc.* **1987**, *109*, 5649.

(42) Resch, U.; Eychmuller, A.; Haase, M.; Weller, H. *Langmuir* **1992**, *8*, 2215.

(43) Hao, E.; Sun, H.; Zhou, Z.; Liu, J.; Yang, B.; Shen, J. *Chem. Mater.* **1999**, *11*, 3096.

(44) Wu, F.; Zhang, J. Z.; Kho, R.; Mehra, R. K. *Chem. Phys. Lett.* **2000**, *330*, 237.

(45) Zhang, J.; Sun, L.; Liao, C.; Yan, C. *Solid State Comm.* **2002**, *124*, 45.

(46) Myung, N.; Bae, Y.; Bard, A. J. *Nano Lett.* **2003**, *3*, 747.

(47) Wankhede, M. E.; Haram, S. K. *Chem. Mater.* **2003**, *15*, 1296.

(48) Mahtab, R.; Rogers, J. P.; Murphy, C. J. *J. Am. Chem. Soc.* **1995**, *117*, 9099.

(49) Lakowicz, J. R.; Gryczynski, I.; Gryczynski, Z.; Nowaczyk, K.; Murphy, C. J. *Anal. Biochem.* **2000**, *280*, 128.

(50) Tian, Y.; Fendler, J. H. *Chem. Mater.* **1996**, *8*, 969.

(51) Moore, D. E.; Patel, K. *Langmuir* **2001**, *17*, 2541.

(52) Li, X.; Coffey, J. L. *Chem. Mater.* **1999**, *11*, 2326.

(53) Hamity, M.; Lema, R. H.; Suchetti, C. A. *J. Photochem. Photobiol. A* **2000**, *133*, 205.

activation has been applied primarily to QDs dispersed in aqueous media,^{41,44,48,52} although it has also been demonstrated in QDs stabilized by surfactants or organic ligands in hydrophobic solvents.^{42,43,53,54} To our knowledge, the present work demonstrates the first example of Cd²⁺ surface activation in QDs decorated by a hydrophobic polymer brush, providing new opportunities for polymeric sensors and devices. With appropriate treatment of the PAA layer, the photoluminescence of these PS-*b*-PAA-stabilized QDs is found to be remarkably stable over periods of several months. We also show that these polymer-coated quantum dots can be well-dispersed in polystyrene homopolymer by simple solution blending, yielding optically clear nanocomposites which retain the photoluminescence of the original colloidal building blocks.

Experimental

Synthesis of Polystyrene-*b*-Poly(Acrylic Acid) (PS-*b*-PAA) Diblock Copolymer. The polystyrene-*b*-poly(*tert*-butylacrylate) diblock copolymer (PS-*b*-P*t*BA) used in the present study was synthesized using well-established anionic polymerization techniques.^{55,56} Therefore, only a brief summary will be presented here. All monomers were stirred over calcium hydride for 24 h, distilled under vacuum, and stored under nitrogen at -20 °C. Before the polymerization reaction, styrene and *tert*-butylacrylate monomers (Aldrich) were further purified by the addition of fluorenyllithium or triethylaluminum, respectively, followed by an additional vacuum distillation step. The tetrahydrofuran (THF) reaction solvent was freshly distilled following reflux over sodium/benzophenone. Solvents, monomers, and initiator were transferred using flamed stainless steel cannulas and syringe needles.

α -Methylstyrene (10–20 drops, Aldrich) were added to a previously flamed reaction flask containing LiCl (10 mol LiCl:1 mol *sec*-butyllithium) dissolved in ca. 450 mL of THF under ultra-high-purity nitrogen atmosphere. The reaction mixture was then titrated with *sec*-butyllithium initiator (1.3 M in hexanes, Aldrich) until a dark red color persisted followed by the addition of the desired quantity of initiator. The reaction flask was cooled to -78 °C using a dry ice/acetone bath followed by the addition of styrene monomer. Once the polymerization of styrene was complete, an aliquot of the reaction mixture was withdrawn for analysis of the degree of polymerization of the polystyrene block by gel permeation chromatography (GPC). The *tert*-butylacrylate monomer was then added to the reaction medium for the polymerization of the second block, after which the polymerization reaction was terminated by the addition of degassed methanol. The *tert*-butylacrylate content of the recovered copolymer was determined using quantitative FTIR spectroscopy of the carbonyl C=O stretching mode from P*t*BA (1730 cm⁻¹) in CCl₄ solution, as previously described.⁵⁶

The block copolymer in the ester form was hydrolyzed to polystyrene-*b*-poly(acrylic acid) (PS-*b*-PAA) by overnight reflux in toluene with *p*-toluenesulfonic acid as the catalyst (5 mol% relative to the *tert*-butylacrylate content), to obtain the block copolymer PS(330)-*b*-PAA(20); the numbers in parentheses indicate degrees of polymerization for each block calculated from number average molecular weights. FTIR confirmed complete hydrolysis; the sharp C=O ester mode at 1730 cm⁻¹ was replaced by a broad acid doublet, which disappeared when the sample was treated with NaOH. The polydispersity of the diblock (P. I. = 1.02) was determined from GPC of the copolymer in the ester form.

Preparation of Polystyrene-*b*-Poly(Cadmium Acrylate) (PS-*b*-PACd) Micelles (MIC-Cd). The block copolymer PS(330)-*b*-PAA(20) was dissolved in benzene/methanol (90:10 v/v) at a concentration of ca. 2 wt%. The formation of reverse micelles with insoluble PACd cores and soluble PS coronae was induced by the addition of excess 0.25 M cadmium acetate dihydrate

(Aldrich) in methanol (1.5 mol cadmium acetate dihydrate:1 mol acrylic acid repeat units) followed by stirring of the solution for 4 h. The material was recovered by freeze-drying then dried in a vacuum oven at 70 °C for 24 h. Excess cadmium acetate was removed by washing the freeze-dried micelles repeatedly with methanol followed by drying the white powder under vacuum at 70 °C for 24 h.

GPC of the resulting PS-*b*-PACd block ionomer in THF (not shown) revealed two fractions: a high-molecular-weight fraction (ca. 70 wt%) attributed to micelles and a low-molecular-weight fraction (ca. 30 wt%) attributed to PS homopolymer resulting from chain termination during anionic polymerization. A fractionation procedure was carried out to remove the PS homopolymer impurity: the sample was dissolved in THF (5 wt%) and stirred at a medium rate while adding deionized water dropwise until a cloudy precipitate persisted that did not redissolve with further stirring. Water addition was stopped before complete precipitation of the sample from THF occurred. The cloudy solution was allowed to settle overnight into two layers. The clear top layer was then separated from the cloudy bottom layer, which was analyzed by GPC to assess the remaining homopolymer content. This procedure was repeated several times until the amount of homopolymer in the bottom layer was <2 wt%. The purified micelle sample was then recovered by precipitation into methanol and dried under vacuum at 70 °C for 24 h.

Preparation of PS-*b*-PAA-Stabilized CdS Quantum Dots (MIC-CdS) and Subsequent Surface Chemistry. Following fractionation, the white powder consisting of PS(330)-*b*-PACd(20) block ionomer micelles was exposed to an atmosphere of 100% humidity for a period of 1 week. The ionomer powder was subsequently exposed to H₂S (bubbled through H₂O at room temperature). After about 45 min, the white powder turned a light yellow color, which intensified with further exposure to H₂S. After 9 h of exposure time, the yellow powder was stored under active vacuum for 12 h to remove excess H₂S. The resulting sample of PS-*b*-PAA-stabilized CdS quantum dots was designated MIC-CdS1.

Various steps of subsequent chemistry in the PAA layer of MIC-CdS1 were carried out to prepare the samples MIC-CdS2, MIC-CdS3, and MIC-CdS4. First, MIC-CdS1 was dispersed in THF (2 wt%) and excess cadmium acetate dihydrate in methanol (2 mol cadmium acetate dihydrate:1 mol acrylic acid repeat units) was added with overnight stirring. A yellow powder was recovered by precipitation into methanol then washed repeatedly with methanol to remove excess cadmium acetate and dried in a vacuum oven at 70 °C for 24 h. This reneutralized sample was designated MIC-CdS2. Second, the yellow powder MIC-CdS2 was exposed to "wet" H₂S (bubbled through H₂O) for 8 h to produce the protonated sample MIC-CdS3. Finally, the PAA layer of MIC-CdS3 was reneutralized with cadmium acetate dihydrate in THF solution and recovered as a yellow powder (MIC-CdS4) as described above for the reneutralization of MIC-CdS1.

The samples MIC-CdS1 and MIC-CdS2 were also treated by titrating with NaOH and cadmium acetate, following aging of each sample dispersed in toluene. For these experiments, colloids of MIC-CdS1 and MIC-CdS2 dispersed in spectroscopic grade toluene were first aged for various periods by storing the solutions in a dark cupboard under ambient conditions and monitoring the photoluminescence and quantum yields at various times as described in the text. After a given period of aging, the solutions were treated with excess NaOH in methanol (4 NaOH:1 acrylic acid repeat unit) and then treated with successively increasing quantities of cadmium acetate dihydrate in methanol until the photoluminescence intensity reached a maximum value.

In addition to the samples MIC-CdS1–MIC-CdS4, an additional QD sample was prepared in a manner identical to that described for MIC-CdS1 but using a different block copolymer, PS(140)-*b*-PAA(17) (Polymer Source, Montreal). This sample was designated MIC-CdS5 and was used for titration experiments comparing the effects of adding cadmium acetate and magnesium acetate on photoluminescence intensity in the band-edge region.

Preparation of QD Blend Films. Blends of MIC-CdS4 and PS homopolymer were prepared by dissolving appropriate quantities of each component in spectroscopic grade toluene to a total polymer concentration of 4 wt%. Two PS homopolymer samples were prepared by anionic polymerization for these

(54) Hamity, M.; Lema, R. H.; Suchetti, C. A. *J. Photochem. Photobiol. A* **1998**, *115*, 163.

(55) Hautekeer, J. P.; Varshney, S. K.; Fayt, R.; Jacobs, C.; Jerome, R.; Teysse, Ph. *Macromolecules* **1990**, *23*, 3893.

(56) Zhong, X. F.; Varshney, S. K.; Eisenberg, A. *Macromolecules* **1992**, *25*, 7160.

blending experiments: PS(1250), P. I. = 1.01, and PS(100), P. I. = 1.04, where the numbers in parentheses indicate degrees of polymerization. Blend solutions were stirred for ~2 h and left to stand overnight in the dark to equilibrate. Solutions were then deposited on 18 mm × 18 mm glass cover slides, placed in Petri dishes covered with aluminum foil, and left in a fumehood to evaporate for 1 week. The resulting CdS QD blend films were then dried overnight in a vacuum oven at 70 °C to remove residual solvent.

Gel Permeation Chromatography (GPC). All GPC measurements were performed using a Viscotek Model 302 liquid chromatography system equipped with refractive index (RI), low-angle light scattering (LALS, $\theta = 7^\circ$), right-angle light scattering (RALS, $\theta = 90^\circ$), and UV detectors. THF was used as the eluent at a flow rate of 1 mL/min, and the column temperature was set at 35 °C. All polymer solutions were filtered through membrane filters with a nominal pore size of 0.45 μm before injection into the GPC column. The data were collected and analyzed on a Dell Dimension 2300 computer with appropriate GPC software from Viscotek. Two ViscoGEL HR High-Resolution Columns (styrene-divinyl benzene columns) in series were used: G3000 HR 60 k GMHHR-M Mixed Bed 4 M columns.

Molecular weights for PS homopolymer and micelle samples were calculated from GPC data using an algorithm from Viscotek, which relies on LALS detection from a 670 nm diode laser source. This utilizes the fundamental Zimm equation for light scattering from polymer solutions:

$$\frac{Kc}{R_\theta} = \frac{1}{M_w P(\theta)} + 2A_2c \quad (1)$$

where R_θ is the excess Rayleigh scattering ratio, $P(\theta)$ is the particle scattering factor, M_w is the weight-average molecular weight of the sample, A_2 is the second virial coefficient, c is the polymer concentration, and K is a composite of optical and fundamental constants. The excess Rayleigh ratio is the ratio of light scattered from the solution in excess of solvent scattering at an angle of detection θ , I_θ , with respect to the incident beam intensity, I_0 : $R_\theta = kI_\theta/I_0$, where k is an instrumental constant. In the typical Zimm plot approach, M_w is analyzed by detecting scattered light for each concentration at a series of angles followed by extrapolation to $\theta = 0$, where the scattering factor $P(\theta) = 1$. In contrast, the present Viscotek LALS monitors light scattered at a single low angle as the sample is eluted; irrespective of particle shape, $P(\theta)$ is very close to 1 for an angle of detection of $\theta = 7^\circ$, so that M_w can be calculated without multi-angle extrapolation. For the CdS-containing samples, A_2 was estimated from multiple injections of the sample MIC-CdS4 at different concentrations.

Absorption and Photoluminescence Measurements. Absorption spectra were recorded on a Cary 50-scan UV-vis spectrophotometer. Static fluorescence measurements were recorded on an Edinburgh Instruments FLS 920 instrument equipped with a Xe 450W arc lamp and a red-sensitive PMT (R928-P). For typical measurements of optical properties, the MIC-CdS samples were dispersed in spectroscopic grade toluene at concentrations such that the measured absorbance at 400 nm was less than 0.1.

Photoluminescence quantum yields (Φ) of the MIC-CdS colloids in toluene were determined using perylene (Aldrich) in deoxygenated absolute ethanol as a reference, which has a fluorescence quantum yield close to 1.0.^{44,57} The following equation was applied

$$\Phi_s = (A_r/A_s)(n_s^2/n_r^2)(D_s/D_r) \quad (2)$$

where A_r and A_s are the absorbance values of the perylene solution and MIC-CdS colloids at 400 nm, respectively, n_s and n_r are the refractive index values of the sample and reference solvents, respectively, and D_s and D_r are the corrected integrated photoluminescence intensities for 400 nm excitation. Before calculating integrated photoluminescence intensities, a solvent background was subtracted and a correction for the detector response was

applied to each sample and reference measurement. However, for simplicity, only the technical spectra are presented in the figures.

Photoluminescence lifetime measurements were performed using an Edinburgh Instruments nF900 nanosecond flashlamp with pulse width 1.0–1.6 ns. All decay profiles were collected until a maximum intensity of 1000 photon counts had been reached. Decay profiles were fitted over two decades of intensity starting at channels after the flashlamp pulse, using a tail-fit algorithm. For band-edge emission, two separate measurements of decay profiles were obtained to determine the error on average lifetimes, and reported fit parameters are averages of the two fits. From repeat measurements, the errors on reported average band-edge lifetimes were between 2 and 10%. For trap emission, the average lifetimes were determined from a single decay profile.

Laser Scanning Confocal Fluorescence Microscopy (LSCFM). Laser scanning confocal fluorescence microscopy measurements of CdS QD blend films were done on a Zeiss LSM 410 equipped with an Ar/Kr laser. All films were excited at ~488 nm, using a band-pass 485 ± 20 nm line selection filter and a FT 510 dichroic beam splitter. A long-pass 515 emission filter was used such that only light above 515 nm reached the PMT. A pinhole diameter of 0.984 Airy Units was used for all measurements, resulting in an optical section thickness of 0.615 μm fwhm.

Transmission Electron Microscopy (TEM). Transmission electron microscopy was performed on a Hitachi H-700 electron microscope, operating at an accelerating voltage of 70 kV. CdS QD blend films were first embedded in an Epon resin, and then 30–60 nm thick sections were produced with a diamond knife on Reichert UltraCut E ultra-microtome. The thin sections were then placed on carbon/Formvar-coated 300 mesh copper grids for imaging.

Dynamic Light Scattering (DLS). Dynamic light scattering (DLS) experiments were carried out on a Brookhaven Instruments photon correlation spectrometer equipped with a BI-200SM goniometer, a BI-9000AT digital autocorrelator, and a Melles Griot He-Ne Laser (632.8 nm) with maximum power output of 75 mW. To ensure the accuracy of DLS measurements, great care was taken to eliminate dust from the samples. Spectroscopic grade toluene was filtered through two membrane filters with 0.20 μm nominal pore size connected in series, and stock solutions of MIC-CdS colloids dispersed in toluene were filtered through two membrane filters with 0.45 μm nominal pore size connected in series. All scintillation vials were thoroughly cleaned with filtered toluene, and stock solutions of the MIC-CdS colloids were filtered into the dust-free scintillation vials. Successive dilutions of the colloids were carried out by adding known quantities of filtered toluene. DLS measurements were conducted at five different angles, 35°, 50°, 70°, 90°, and 120°, and at five different concentrations in the range of 0.05–0.01 mg/mL. For each angle and concentration, three repeat measurements of the autocorrelation function were obtained. All DLS measurements were conducted at 23 °C.

Results and Discussion

Absorption and FTIR Spectra of PS-*b*-PAA-Stabilized CdS QDs: Effect of Surface Chemistry. H₂S treatment of the freeze-dried PS(330)-*b*-PACd(20) micelles (MIC-Cd) yielded a yellow powder (MIC-CdS1) that could be easily dispersed in various organic solvents (e.g., toluene, chloroform, THF) to obtain clear yellow solutions. The structured absorption spectrum of MIC-CdS1 in toluene (Figure 1) allows optical transitions at 428 and 378 nm to be distinguished, indicating low-polydispersity quantum-confined CdS. From the position of the absorption edge (474 nm), a CdS nanoparticle diameter of 44 Å is calculated using Henglein's empirical curve relating the absorption threshold and CdS QD size.⁶

Previous work on CdS QD synthesis in block ionomers suggested the formation of a single QD in each block ionomer microdomain, pointing to a mechanism of nanoparticle size control via the aggregation number of the original block ionomer template.³⁰ In the present case, we

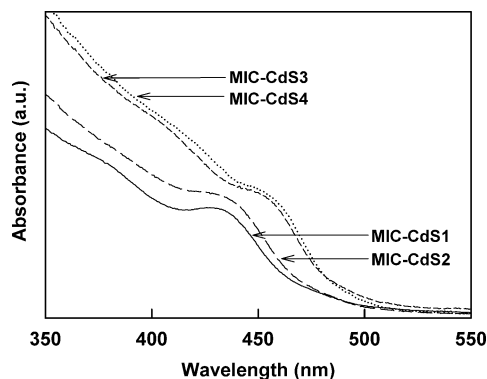


Figure 1. Absorption spectra of PS-*b*-PAA-stabilized CdS QDs in toluene with various treatments of the PAA layer.

determined the micelle aggregation number of MIC-Cd dispersed in THF to be ~ 100 , using GPC with LALS detection. Considering that each PAA block contains 20 units of acrylic acid, the number of Cd^{2+} ions in the micelle core is therefore ~ 1000 , assuming bridged Cd^{2+} counterions following neutralization with cadmium acetate. We point out that actual aggregation numbers following freeze-drying from benzene/methanol may be somewhat different from values determined in THF due to differences in solvent polarity, although on the basis of earlier small-angle X-ray scattering results,⁵⁸ this effect is not expected to be large. Assuming the bulk CdS density value ($d = 4.82 \text{ g/mL}$), the number of Cd^{2+} ions in each 44 \AA nanoparticle of MIC-CdS1 is ~ 900 , in good agreement the original number of Cd^{2+} ions in the ionomer template; this indicates that a single CdS QD is formed in each micelle core. The proposed structure for the MIC-CdS1 particles is shown in Scheme 1, indicating a single CdS QD coated by a layer of PS-*b*-PAA chains. The PS blocks provide solubility in organic solvents and the reactive PAA layer at the polymer-inorganic interface provides a route to further chemistry at the QD surface.

The PAA interface layer of MIC-CdS1 was subsequently treated with successive reneutralization/reprotonation steps to yield MIC-CdS2–MIC-CdS4, as shown in Figure 2A. All four samples were isolated as bright yellow powders that could be dispersed in various organic solvents to yield optically clear yellow solutions. Following each step of chemical treatment at the QD surface (Figure 2A), an FTIR spectrum was obtained to characterize the PAA layer (Figure 2B). For MIC-CdS1, the C=O stretching vibration results in a broad band at 1710 cm^{-1} with a shoulder at $\sim 1738 \text{ cm}^{-1}$. This doublet absorption band is characteristic of carboxylic acid groups and confirms that H_2S treatment of the original block ionomer template resulted in reprotonation of the PAA blocks, forming COOH groups in the interface layer of MIC-CdS1. Treatment of MIC-CdS1 by stirring in THF with an excess of cadmium acetate, followed by washing to remove residual cadmium acetate, results in a disappearance of the C=O carboxylic acid doublet and appearance of a band at $\sim 1550 \text{ cm}^{-1}$, attributed to asymmetric stretch of COO^- in PACd; this suggests that the carboxylate groups in the interface layer are neutralized with Cd^{2+} counterions in MIC-CdS2. Subsequent treatment of MIC-CdS2 with H_2S results in a return of the carboxylic acid doublet and nearly complete disappearance of the 1550 cm^{-1} band, indicating reprotonation of the PAA layer in MIC-CdS3. Finally, another treatment with excess cadmium acetate reneutralizes the acid layer at the QD surface, as shown by a return of the

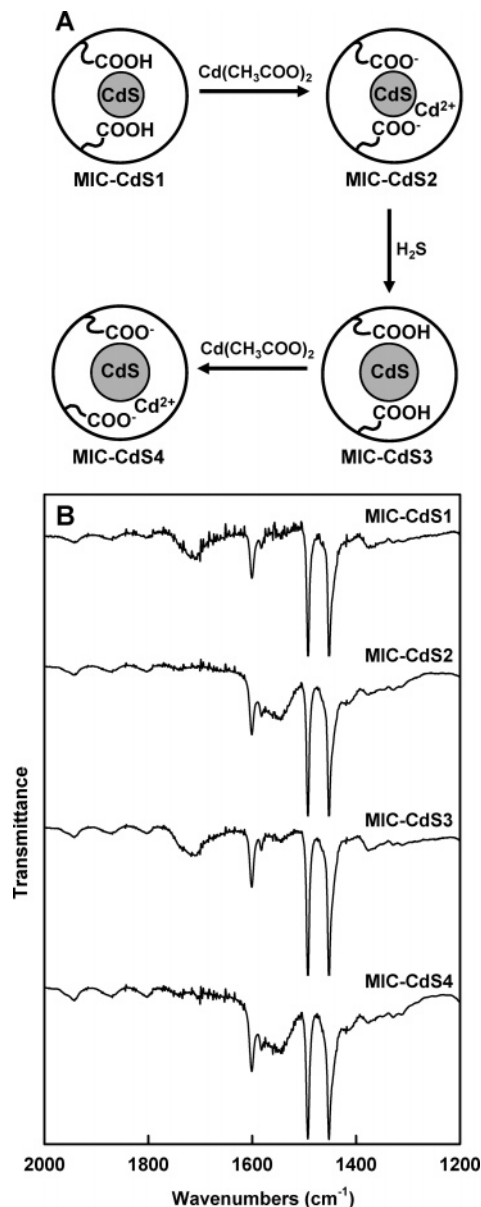


Figure 2. Schematic demonstrating various treatments of PS-*b*-PAA-stabilized CdS QDs and effect on QD size and PAA layer (A) and FTIR spectra of the resulting four samples (B).

1550 cm^{-1} band and nearly complete disappearance of the acid doublet in MIC-CdS4.

Comparison of absorption spectra of MIC-CdS1–MIC-CdS4 in toluene reveals the effect of chemical treatment of the PAA interfacial layer on the QD size (Figure 1). The CdS spectrum of MIC-CdS2 shows a marginal red-shift relative to MIC-CdS1, indicating a slight increase in QD diameter from 44 to 47 \AA , which is attributed to ripening during cadmium acetate treatment in THF solution. A more marked change in the absorption spectrum is observed for MIC-CdS3 following H_2S treatment of MIC-CdS2, with a red-shift in the absorption edge to 492 nm , corresponding to an increase in the CdS nanoparticle size to 54 \AA . This size increase is explained by secondary growth of the QDs by deposition of CdS on the surface of the original nanoparticles. Subsequent reneutralization of the PAA layer does not result in a significant change in the QD size, as indicated by the nearly overlapping absorption spectra of MIC-CdS3 and MIC-CdS4.

Surface-Tunable Photoluminescence of PS-*b*-PAA-Stabilized CdS QDs. Along with the well-estab-

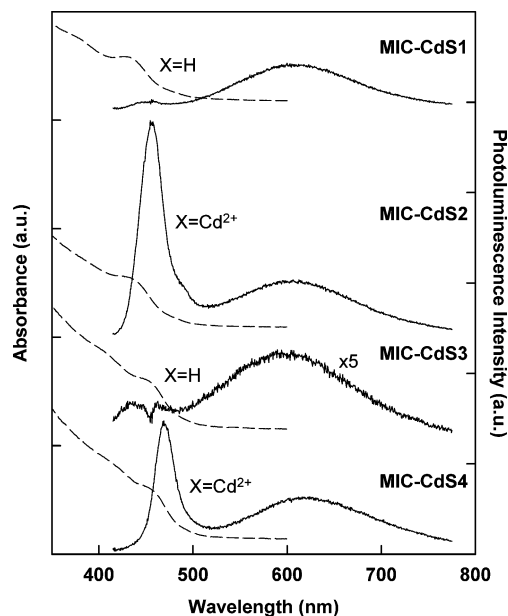


Figure 3. Absorption and photoluminescence emission spectra ($\lambda_{\text{ex}} = 400$ nm) for the four PS-*b*-PAA-stabilized CdS QDs samples in toluene. The chemical form of the PAA layer is denoted COOX, where X = H or Cd²⁺.

lished effects of quantum confinement, the photoluminescence of semiconducting QDs is strongly dependent on the presence of surface states due to the large percentage of surface atoms in these systems. The presence of these surface states allows the photoluminescence to be modified by chemical interactions between semiconductor surface sites and an organic or inorganic passivating layer.^{2-6,9,41,42} In the present case of block copolymer-encapsulated QDs, the interfacial PAA layer can be varied between protonated and Cd²⁺-neutralized forms following synthesis of the QD, providing a convenient handle on postsynthesis tuning of QD photoluminescence without affecting the external PS functionality, via the nature of interactions between PAA and the CdS surface.

The effect of chemical treatment of the PAA layer on QD photoluminescence is clearly demonstrated in Figure 3, which compares the photoluminescence emission spectra of the four samples MIC-CdS1–MIC-CdS4 dispersed in toluene solutions. All QD solutions were prepared with optical densities <0.1 at 400 nm to ensure that auto-absorption effects were negligible. MIC-CdS1 shows a broad red-shifted emission band centered at 613 nm, which is attributed to recombination from a distribution of deep trap states localized at the QD surface.^{41,42,52} A very weak band-edge emission (455 nm) is also visible, attributed to recombination from band-edge or near-band-edge states. The low intensity of band-edge emission compared to trap-state emission suggests a high density of surface trap states in MIC-CdS1 and a correspondingly high probability of crossover to these traps once an exciton is created by light absorption.

A dramatic increase in the relative intensity of band-edge emission is seen following conversion of the PAA layer to its cadmium carboxylate form in MIC-CdS2, suggesting a decrease in the density of trap states via changes in interactions between the PAA layer and the QD surface (Figure 3). In Figure 4, it is evident that the position and shape of the narrow and broad bands were unchanged when emission spectra of MIC-CdS2 were obtained at different excitation wavelengths from 350 to 425 nm, a further indication of a narrow QD size distribution. Normalized excitation spectra of MIC-CdS2

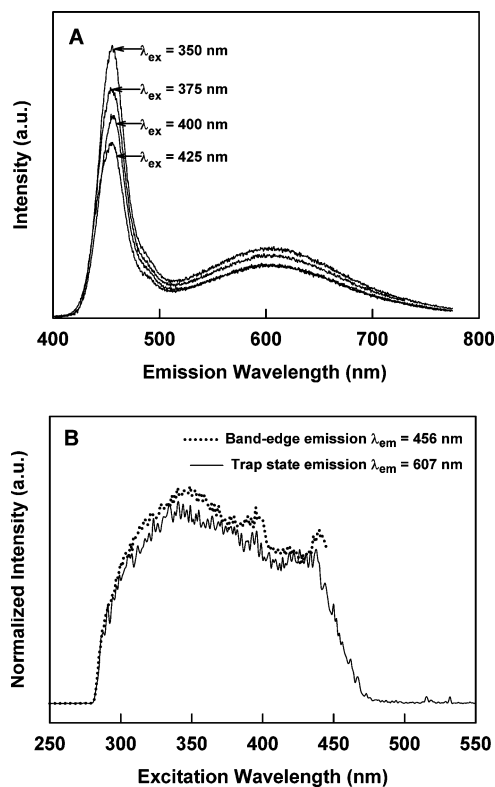


Figure 4. Photoluminescence emission spectra of MIC-CdS2 in toluene with various excitation wavelengths (A) and excitation spectra of MIC-CdS2 in toluene with emission wavelengths corresponding to the band-edge and trap-state emission maxima (B).

Table 1. Relative Quantum Yields for Block Copolymer-Stabilized CdS Quantum Dots in Toluene with Various Treatments of the PAA Layer

sample	QD diameter (Å) ^a	PAA layer		ϕ^b
		COOX	X = H, Cd ²⁺	
MIC-CdS1	44	H		0.019
MIC-CdS2	47	Cd ²⁺		0.030
MIC-CdS3	54	H		0.006
MIC-CdS4	54	Cd ²⁺		0.018

^a Determined from UV–vis absorption edge. ^b Quantum yield values determined at $\lambda_{\text{ex}} = 400$ nm using perylene in ethanol as a reference.

obtained for emission wavelengths corresponding to the maxima of the narrow and broad bands show excellent overlap (Figure 4B), confirming that band-edge and trap-state emission originate from equivalent initial excited states. Comparison of photoluminescence quantum yields (Table 1), shows that the conversion of the PAA layer to its cadmium carboxylate form resulted in an overall 50% enhancement in the quantum yield of MIC-CdS2 compared with MIC-CdS1, consistent with a decrease in the density of deep trap states, from which nonradiative processes are dominant.

H₂S treatment of MIC-CdS2, along with increasing the QD size, was found to reverse the effects of Cd²⁺-neutralization on the photoluminescence, resulting in a sharp drop in the band-edge emission for MIC-CdS3 (Figure 3) and an overall decrease in the quantum yield (Table 1). The band-edge emission was shown to be reactivated by again neutralizing the PAA layer with cadmium acetate, increasing the quantum yield of MIC-CdS4 by a factor of 2 relative to MIC-CdS3. Both band-edge (469 nm) and trap-state (622 nm) emission bands in MIC-CdS4 are red-shifted relative to the corresponding

bands in MIC-CdS2, consistent with the increase in QD size by CdS deposition on the surface of the original nanoparticle. We note that the quantum yield of MIC-CdS3 (0.006) is lower than the quantum yield of MIC-CdS1 (0.019), despite the fact that the PAA layer is in the acid form in both of these samples; as well, activation of MIC-CdS3 by cadmium acetate treatment results in a quantum yield for MIC-CdS4 (0.018) that is lower than the value for Cd²⁺-neutralized MIC-CdS2 (0.030). The lower quantum yields of MIC-CdS3 and MIC-CdS4 compared with MIC-CdS1 and MIC-CdS2, respectively, suggest the formation of new surface trap states during deposition of the outer CdS layer, as well as the possible formation of defect-related traps localized below the nanoparticle surface.

Spanhel et al. proposed that surface activation of colloidal QD photoluminescence with Cd²⁺ addition at high pH is due to the passivation of hole traps localized at anionic sulfide groups at the nanoparticle surface.⁴¹ A similar argument can be applied to the present case, where surface activation is facilitated by the chemical reactivity of the hydrophilic PAA layer. When the PAA is in its protonated form, only H-bonding interactions are possible between COOH groups in the PAA layer and SH⁻ anions at the CdS nanoparticle surface; these interactions are not effective in passivating the SH⁻ surface traps,^{42,52} resulting in a high percentage of trap state emission in MIC-CdS1 and MIC-CdS3. When the PAA layer is treated with cadmium acetate, the COOH groups in the PAA layer are deprotonated, along with some of the SH⁻ sites at the nanoparticle surface, creating S²⁻...Cd²⁺...-OOC structures between the QD and PAA layer. These are similar to the S²⁻...Cd²⁺...-OH surface structures proposed by Spanhel et al.,⁴¹ which lower the density of trap states through passivation of the anionic sulfide sites, decreasing the probability of exciton localization at the surface traps. Cadmium acetate treatment therefore results in activated QDs (MIC-CdS2 and MIC-CdS4) with enhanced band-edge emission and higher quantum yields. The maximum quantum yield we have measured in our activated samples thus far is $\phi \approx 0.04$, lower than the $\phi > 0.50$ values that have been observed in systems of CdS activated in aqueous colloids,⁴¹ although significantly higher than values for typical unpassivated CdS and CdSe nanoparticles in which trap emission dominates ($\phi < 0.001$).^{44,59}

The demonstrated “switching” between activated and nonactivated QD photoluminescence by alternating the interfacial PAA layer between acid and cadmium carboxylate forms points to possible sensor applications for these polymer-coated QDs. The sensitivity of QD photoluminescence to surface states has led to proposed applications of QDs as luminescent sensors for specific analytes, including H⁺, Cd²⁺, Zn²⁺, Cu²⁺, I⁻, oxygen, and DNA, via activating or quenching interactions with the QD surface.^{48,49,60} To our knowledge, this is the first example of Cd²⁺-activation in a system of hydrophobic, polymer-brush-coated QDs, made possible by the reactive and hydrophilic PAA layer which both concentrates Cd²⁺ at the QD surface and contributes to the resulting passivating surface structures. We note that the PS exterior of these particles allows for easy processing via organic solvent casting to obtain optically clear and mechanically stable thin films.³⁰ In light of the present observations, such fluorescent polymer-QD films should have interesting potential as sensitive probes for Cd²⁺

Table 2. Results of Two- and Three-Exponential Fits of Photoluminescence Intensity Decay Profiles for Band-Edge and Trap-State Emission

sample	λ_{em} (nm) ^a	number of exponential terms	$\bar{\tau}$ (ns) ^b	χ^2
MIC-CdS1	613	3	244	1.01
MIC-CdS2	456	2	49	1.17
	607	3	360	1.11
MIC-CdS3	461	2	61	1.02
	610	3	324	1.15
MIC-CdS4	469	2	40	1.10
	622	3	272	1.06

^a For all decay profiles, $\lambda_{ex} = 400$ nm. ^b Intensity-average lifetimes calculated from two- or three-exponential fits (see text).

and other analytes that activate or quench QD photoluminescence.

Further insight into the nature of the emitting states in these QD samples was obtained from decays of the emission intensity, measured at emission wavelengths corresponding to the maxima of the narrow and broad bands. As previously observed for other QD lifetime measurements,^{44,48,49,53,54,61,62} none of the emission profiles could be fitted to single-exponential decays, reflective of a distribution of states and QD sizes within both bands. Decay profiles were therefore fitted to a multiexponential model:

$$I(t) = \sum_i \alpha_i \exp(-t/\tau_i) \quad (3)$$

where two and three exponentials were used to fit band-edge and trap-state emission, respectively, obtaining $\chi^2 \leq 1.2$ for all fits. It is important to note that the lifetimes of individual exponential components for these fits do not correspond to the lifetimes of actual states but rather are used to represent average lifetimes for a broad distribution of states. We therefore report intensity-average lifetimes $\bar{\tau}$ ⁶³ in Table 2, determined from the results of two- or three-exponential models using

$$\bar{\tau} = \frac{\sum_i a_i \tau_i^2}{\sum_i a_i \tau_i} \quad (4)$$

Representative intensity decay profiles for band-edge and trap-state emission are compared in Figure 5, showing that the broad red-shifted emission decays with a significantly longer lifetime than the band-edge emission, as has been found in other examples of Cd²⁺-activated CdS.^{48,49} The relatively long lifetimes for the red-shifted emission band (244–360 ns) supports the assumption that this band originates from localized deep trap states. The measured band-edge lifetimes (40–61 ns), though shorter than those for the red-shifted emission band, are much

(61) Wang, X.; Qu, L.; Zhang, J.; Peng, X.; Xiao, M. *Nano Lett.* **2003**, *3*, 1103.

(62) Wuister, S. F.; Swart, I.; van Driel, F.; Hickey, S. G.; de Mello Donega, C. *Nano Lett.* **2003**, *3*, 503.

(63) We point out that these average lifetimes were obtained using a total of 1000 counts; we acknowledge that this is not ideal, although unfortunately, extremely long collection times (up to 8 h for 1000 counts) made collecting 10 000 counts prohibitive for these samples. We point out that we are only fitting our data over two decades of time, and from Table 2 it is clear that good fits are obtained in this region. As well, we are only reporting average lifetimes from the fits, and these values are quite reproducible for repeat measurements, with errors of ~2% for most samples, despite somewhat nonideal total counts.

(59) Joo, J.; Na, H. B.; Yu, T.; Yu, J. H.; Kim, Y. W.; Wu, F.; Zhang, J. Z.; Hyeon, T. *J. Am. Chem. Soc.* **2003**, *125*, 11100.

(60) Chen, Y.; Rosenzweig, Z. *Anal. Chem.* **2002**, *74*, 5132.

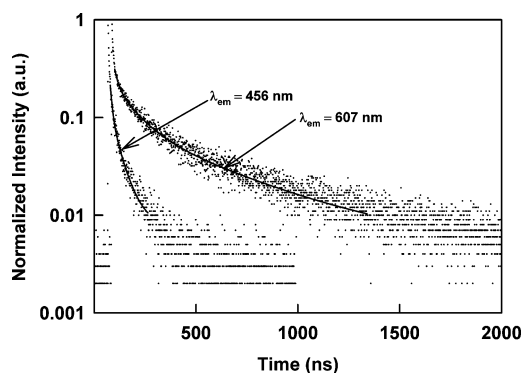


Figure 5. Comparison of band-edge ($\lambda_{em} = 456$ nm) and trap-state ($\lambda_{em} = 607$ nm) emission decay profiles for MIC-CdS2 in toluene and resulting two- and three-exponential fits, respectively.

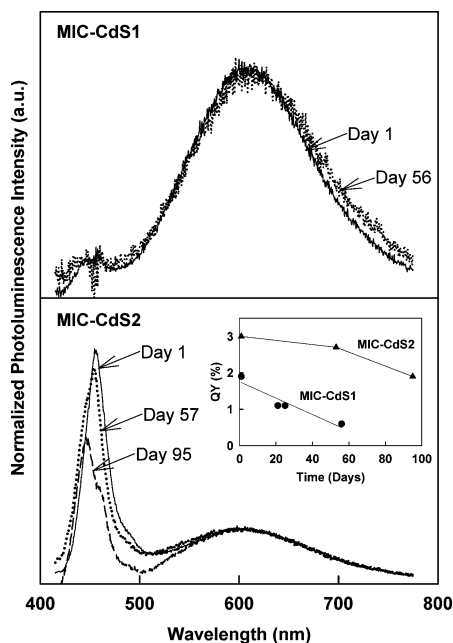


Figure 6. Photoluminescence emission spectra ($\lambda_{ex} = 400$ nm) of MIC-CdS1 and MIC-CdS2 in toluene after various periods of aging under ambient conditions. The emission spectra have been normalized to allow comparison of relative intensities of band-edge and trap-state emission. The measured quantum yields at various times are shown in the insert.

longer than the picosecond lifetimes which have been measured for direct band-edge recombination of an exciton.^{41,44} This suggests that a significant amount of band-edge emission in this system is actually due to recombination from shallow trap states located close to the band edge, as has been observed for other systems.^{41,44} We note that picosecond processes may also contribute to the band-edge emission, though these cannot be resolved due to limitations in the instrument response time.

The long-term solution stability of the photoluminescence properties was investigated for both nonactivated (MIC-CdS1) and activated (MIC-CdS2) samples stored under ambient conditions. The photoluminescence spectra and quantum yields for the two samples were monitored over time following dispersion of the yellow powders in toluene (Figure 6). To better compare the relative intensities of band-edge and trap-state emission, the emission spectra collected at various times are normalized, with the respective quantum yields shown in the insert. For MIC-CdS1, the shape of the dominant broad trap emission does not change considerably over 56 days, indicating that

the nature of the surface states remain constant. However, the quantum yield decreases by a factor of 3 over this same time period, suggesting an increase in nonradiative recombination pathways for the surface traps as the particles age in toluene. The activated sample, MIC-CdS2, along with having a higher initial quantum yield, shows a much greater stability than MIC-CdS1, maintaining 90% of its photoluminescence after 57 days in toluene solution. Over this time period, the shape of the broad trap-state emission remains constant, although the band-edge emission shows a slight blue-shift and decrease in intensity relative to the trap state emission. After 95 days in toluene, the band-edge emission of MIC-CdS2 decreases more significantly, with a concomitant decrease in the quantum yield. These observations are consistent with the slow oxidation of the activated QD surface of MIC-CdS2 over long periods of time in toluene solution. Surface oxidation of QDs is a well-established mechanism of nanoparticle degradation and has been found to result in a decrease in QD size and increase in the density of surface traps by the formation of new anionic sulfide sites.^{3,64} For typical TOPO-stabilized QDs exposed to air, the dramatic loss of photoluminescence intensity due to nanoparticle degradation is an extremely rapid process, occurring over the course of several minutes.⁶⁴ The impressive degree of stability for MIC-CdS2 over several months of aging in toluene is therefore very encouraging, pointing to the protective nature of the polymer layer.

After MIC-CdS1 and MIC-CdS2 were aged in toluene, we found that the original photoluminescence properties of the QDs could be restored, and even enhanced, by direct activation of the aged toluene solutions. For these experiments, the aged QD solutions in toluene were first titrated with an excess of $4\times$ NaOH in methanol (relative to the number of acrylic acid units) followed by titration with cadmium acetate in methanol until the quantum yield of the solution reached a maximum value (Figure 7). The aged nonactivated sample MIC-CdS1 showed only weak broad trap emission before NaOH addition, with even weaker band-edge emission ($\phi = 0.06$) (Figure 7A). Addition of excess NaOH resulted in a small increase in band-edge emission. This small activation effect is not attributed to Na_2S deposition on the QD surface, which has been found to quench, rather than activate, photoluminescence;⁵⁴ rather, we believe that a small number of SH^- sites were passivated by deprotonation with NaOH followed by reaction with Cd^{2+} ions that had been released into the PAA layer during QD surface oxidation.⁶⁴ Subsequent addition of Cd^{2+} ions resulted in a steady increase in both band-edge and trap-state emission, until a maximum quantum yield of 0.037 was obtained for the originally nonactivated MIC-CdS1. The increase in trap-state emission suggests that the formation of an increasing number of passivating groups on the QD surface, along with lowering the density of trap states, also increases the amount of radiative recombination from the remaining traps, as was found in the activation experiments of Spanhel et al.⁴¹

A similar effect was found for the aged activated sample MIC-CdS2, which had lost much of its original photoluminescence intensity due to surface oxidation during 95 days in toluene ($\phi = 0.019$). In this case, the initial addition of NaOH was found to quench the photoluminescence (Figure 7B), though subsequent titration with Cd^{2+} resulted in an increase in activation until the quantum yield reached 0.036. The observed quenching with NaOH

(64) Derfus, A. M.; Chan, W. C. W.; Bhatia, S. N. *Nano Lett.* **2004**, *4*, 11.

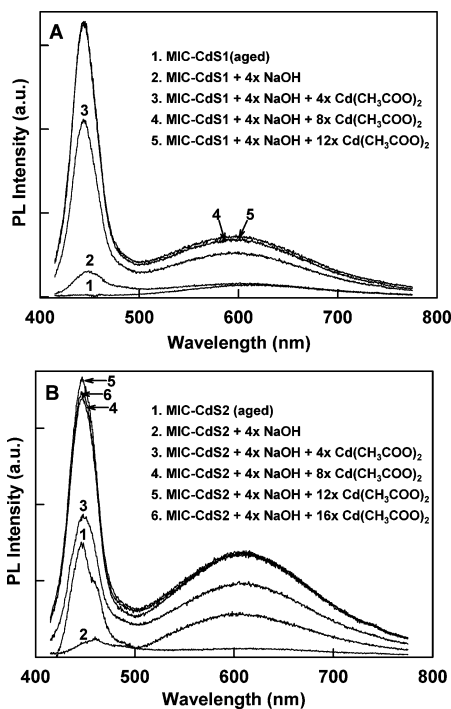


Figure 7. Photoluminescence emission spectra ($\lambda_{\text{ex}} = 400$ nm) of aged MIC-CdS1 (A) and MIC-CdS2 (B) in toluene with various subsequent treatments of added NaOH and $\text{Cd}(\text{CH}_3\text{COO})_2$ in methanol.

addition is explained in terms of the large excess of Na^+ ions, which can displace Cd^{2+} ions from passivating $\text{S}^{2-}\cdots\text{Cd}^{2+}\cdots\text{OOC}$ structures at the QD surface.⁵⁴ As well, we note that after the maximum quantum yield was obtained, subsequent addition of cadmium acetate resulted in a slight decrease in the band-edge emission. This was probably due to a competing quenching effect associated with the added methanol since hydrogen bonding is known to compete with passivating interactions with trap sites on the surface of CdS.^{42,51}

To demonstrate the selectivity of PS-*b*-PAA-stabilized QDs as chemical sensors for Cd^{2+} ions, we compared the effects of adding increasing quantities of cadmium or magnesium acetate to toluene QD solutions on the photoluminescence activation of the band-edge emission region. The results in Figure 8 were obtained from two separate solutions of identical concentration of the sample MIC-CdS5; in both the cadmium and magnesium acetate titration experiments, curve 1 represents the original untreated sample in the protonated form and curve 2 represents the sample after the addition of $4\times$ NaOH in methanol. Curves 3–6 clearly show the effects on each QD solution of the further addition of identical quantities of methanolic solutions of cadmium (above) or magnesium (below) acetate. Whereas cadmium acetate addition results in a progressive increase in the intensity of band-edge emission, magnesium acetate shows no such effect, suggesting that this is an ion-selective activation effect, in agreement with the mechanism proposed above.

Effect of Surface Chemistry on the Solution Structure of PS-*b*-PAA-Stabilized QDs. We found that all four samples MIC-CdS1–MIC-CdS4 could be dispersed in various organic solvents, including toluene, tetrahydrofuran (THF), and chloroform, to yield stable clear yellow solutions that showed no precipitation over a time period of up to several months. This indicated that all PS-*b*-PAA-stabilized QD samples were solubilized and well-stabilized by the PS brush layer, irrespective of the chemical form of the PAA layer. However, we were

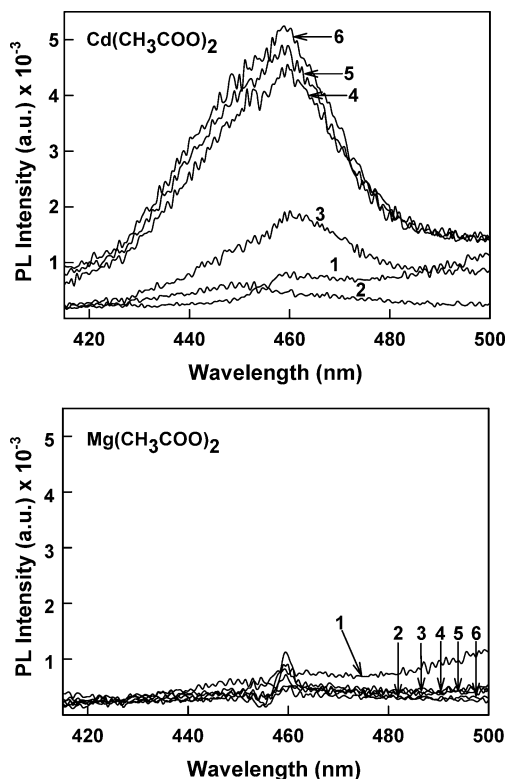


Figure 8. Comparison of photoluminescence emission ($\lambda_{\text{ex}} = 400$ nm) in the band-edge region for MIC-CdS5 in toluene with the addition of increasing amounts of cadmium or magnesium acetate. 1, untreated MIC-CdS5; 2, MIC-CdS5 + $4\times$ NaOH; 3, MIC-CdS5 + $4\times$ NaOH + $4\times$ $\text{M}(\text{CH}_3\text{COO})_2$; 4, MIC-CdS5 + $4\times$ NaOH + $8\times$ $\text{M}(\text{CH}_3\text{COO})_2$; 5, MIC-CdS5 + $4\times$ NaOH + $12\times$ $\text{M}(\text{CH}_3\text{COO})_2$; 6, MIC-CdS5 + $4\times$ NaOH + $16\times$ $\text{M}(\text{CH}_3\text{COO})_2$; $\text{M} = \text{Cd}^{2+}$ (above) or Mg^{2+} (below).

interested in determining more precisely the structure of our polymer-coated QDs in organic solvents and how their solution structure was influenced by the nature of the PAA layer. It has previously been found for polystyrene-*b*-poly(methacrylic acid) (PS-*b*-PMMA) block ionomers that micelle aggregation numbers are significantly higher when the PMMA block is in its neutralized form due to a greater difference in the solubilities of the two blocks.⁶⁵ Moreover, a combination of GPC and dynamic light scattering results suggest that protonated PS-*b*-PMMA⁶⁵ and PS-*b*-PAA⁵⁶ diblocks exist as molecularly solubilized single chains in hydrogen-bonding solvents such as THF due to favorable interactions between the solvent and the acid block and a correspondingly low driving force for micellization. In light of the latter observation, it is perhaps surprising that our acid-form QD samples (MIC-CdS1 and MIC-CdS3) are stable in THF since solubility differences alone may not be sufficient to maintain the encapsulating micelle structure.

Further insight into this question is obtained from GPC of the four samples, in which LALS detection allows the apparent molecular weight of the samples to be determined without reference to standard calibration, by measuring the scattered light intensity at a single low angle ($\theta = 7^\circ$) as the sample is eluted from the column. For these calculations, we used the dn/dc value for polystyrene in THF, 0.185, since the effects of chemical heterogeneity will be small considering the low weight fraction of the PAA and CdS components (< 10 wt%). The RI-GPC traces for the four samples in THF solution are shown in Figure

(65) Desjardins, A.; van de Ven, Th. G. M.; Eisenberg, A. *Macromolecules* **1992**, *25*, 2412.

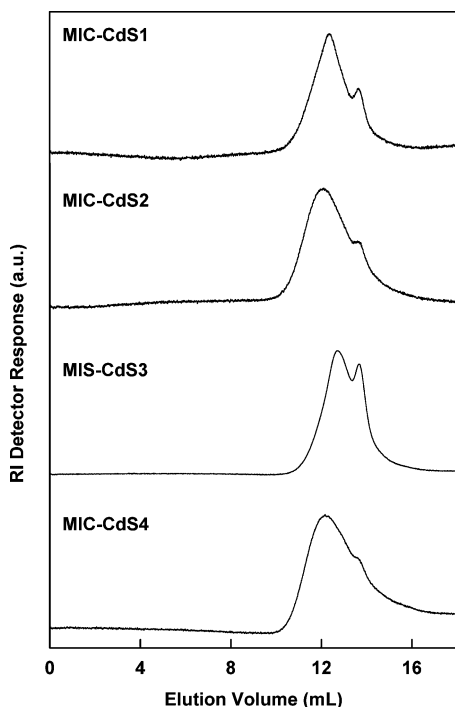


Figure 9. Gel permeation chromatograms (refractive index detector response) for the four samples of PS-*b*-PAA-stabilized CdS QDs in THF.

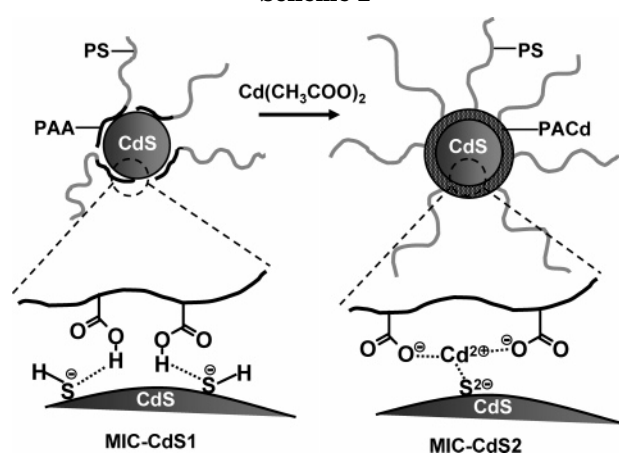
Table 3. Weight-Average Molecular Weights and Block Copolymer Aggregation Numbers, *Z*, of PS-*b*-PAA-Stabilized CdS Quantum Dots in THF

sample	M_w (g/mol) $\times 10^{-6}$ ^a	<i>Z</i>
MIC-Cd	3.49	96
MIC-CdS1	0.90	24
MIC-CdS2	3.84	105
MIC-CdS3	0.75	20
MIC-CdS4	3.81	104

^a Determined using GPC from RI and LALS detector signals as described in the text.

9. All four samples show a relatively broad peak, attributed to the polymer-coated QDs, along with a low-molecular-weight shoulder. This shoulder was not sufficiently resolved to determine its molecular weight independently, although its elution volume matched perfectly with the original unmicellized ester form of the PS(330)-*b*-PtBA-(20) copolymer; it was therefore attributed to a “single chain” fraction within each sample. We note that the single chain shoulder is significantly sharper in MIC-CdS1 and MIC-CdS3 compared with that of MIC-CdS2 and MIC-CdS4, suggesting a larger fraction of unassociated single chains when the PAA layer is in its acid form. More compelling evidence came from the determination of the weight-average molecular weights for each sample by integrating the RI and LALS traces for each of the broad peaks. Table 3 shows the resulting M_w and average block copolymer aggregation numbers, *Z*, for MIC-CdS1–MIC-CdS4, as well as values for the original cadmium-neutralized micelles. For all of the cadmium-neutralized samples, including the original block ionomer micelles, *Z* values are in the range of 96–105, while for the two QD samples in which the PAA layer is in its acid form (MIC-CdS1 and MIC-CdS3), *Z* values are about a factor of 5 lower, in the range of 20–24, consistent with the observed larger fraction of single chains in these samples. For one of our samples, MIC-CdS4, we have also carried out multi-angle static light scattering measurements in THF to compare the more-typical Zimm plot method with the

Scheme 2



LALS–GPC results. The Zimm plot method gives an aggregation number of ~ 320 in THF, which is about a factor of 3 greater than the value obtained by LALS–GPC. The reason for this discrepancy is unclear at present, although one explanation is that a fraction of large supermicellar aggregates in THF contribute to the average molecular weight as determined by the Zimm plot method; these aggregates may be retained by the column and so are not detected by the GPC method.

Considering the similar aggregation numbers determined by LALS–GPC for all of the cadmium-neutralized samples, it is reasonable to propose that chain aggregation in these cases is driven by the low solubility of the PACd blocks in THF. The lower aggregation numbers for MIC-CdS1 and MIC-CdS3 could then be explained by a greater solubility of the single chains in their acid form and a correspondingly lower tendency to form micelles. However, in previous studies of PS-*b*-PMAA⁶⁵ and PS-*b*-PAA⁵⁶ with relatively short acid blocks, reverse micelles were not observed in THF for the copolymers in the acid form. It is therefore possible that chain aggregation about the CdS QDs in MIC-CdS1 and MIC-CdS3 is not driven by solubility differences between the PAA blocks but by H-bonding interactions between the PAA blocks and SH[−] groups at the QD surface. Compelling support for this model comes from a calculation of the number of sulfur atoms on the surface of a 44 Å QD in MIC-CdS1, determined to be 364, assuming bulk CdS density and 3.5 Å for a CdS monolayer.⁶⁶ This agrees very well with chain aggregation numbers ($Z \approx 20$) determined from LALS–GPC for these structures, which for a 20 unit PAA block would result in ~ 400 COOH groups at the QD surface. Comparison of the proposed structures for MIC-CdS1 and MIC-CdS2 in THF is shown in Scheme 2. In this cartoon, all of the chains in the PAA layer of MIC-CdS1 interact directly with the QD surface through H-bonding. In contrast, when the PAA layer is in its neutralized form, a thicker PACd layer forms around the QD, driven by microphase-separation of the insoluble ionic blocks. In the latter case, the QDs can be said to be embedded in the core of an ionomer micelle, the structure of which is maintained by interfacial tension between PACd and solvent. Similar differences in aggregation numbers should exist in other organic solvents, although aggregation numbers may be somewhat higher in less-polar solvents.⁶⁵ The thicker PACd layer surrounding the QDs in MIC-CdS2, compared with the H-bonded PAA layer in MIC-CdS1 (Scheme 2), may in part explain the greater long-term photoluminescence

(66) Peng, X.; Schlamp, M. C.; Kadavanich, A. V.; Alivisatos, A. P. *J. Am. Chem. Soc.* **1997**, *119*, 7019.

Table 4. Summary of Dynamic Light Scattering Results for Various Block Copolymer-Stabilized CdS Quantum Dots in Toluene

sample	D_0 (nm ² s ⁻¹) × 10 ⁻⁷	r_h (nm)	$\mu_2/\bar{\Gamma}^{2a}$	k_d (cm ³ g ⁻¹)
MIC-CdS1	2.13	18	0.29	-0.00118
MIC-CdS2	1.65	23	0.20	-0.00054
MIC-CdS3	1.32	29	0.28	-0.00006
MIC-CdS4	1.03	37	0.15	-0.00014

^a Polydispersity values averaged over all concentrations and angles for each sample.

stability in the former sample due to protection of the QD surface with a stable and continuous polymer layer which is kinetically “locked in” by the high T_g of PACd.

To obtain further structural information on the polymer-coated QDs in organic solvents, we carried out DLS measurements for all four samples in toluene solutions over a range of scattering angles and concentrations. For all measurements, the normalized time correlation function of the electric field was analyzed using a cumulant expansion:

$$|g(\tau)| = \exp(-\bar{\Gamma}\tau)[1 + (\mu_2/2!)\tau^2 + \dots] \quad (5)$$

where $\bar{\Gamma}$ is the mean relaxation rate and μ_2 is the second moment. Mean relaxation rates were determined for various scattering angles between 35° and 120°, and the effective translational diffusion coefficient, D_T , was determined using the following relation for diffusive motion of particles:

$$\bar{\Gamma} = D_T q^2 \quad (6)$$

where q is the scattering vector, which is related to the refractive index of the scattering medium, n , the wavelength of incident light, λ , and the scattering angle, θ , by the following relation:

$$q = (4\pi n/\lambda) \sin(\theta/2) \quad (7)$$

To correct for interparticle interactions, the effective diffusion coefficient at various concentrations was extrapolated to infinite dilution to obtain D_0 :

$$D_T = D_0(1 + k_d c) \quad (8)$$

where k_d is the concentration coefficient and c is the concentration. From D_0 , the hydrodynamic radius, r_h , of the particles could then be determined from the Stokes–Einstein relation:

$$r_h = kT/6\pi\eta D_0 \quad (9)$$

where k is the Boltzmann constant, T is the temperature, and η is the solvent viscosity. We note that r_h determined by DLS is an inverse reciprocal z average of the distribution of particle sizes, which follows from the scattering intensity-weighting of the diffusion coefficient.

For each cumulant fit, the ratio $\mu_2/\bar{\Gamma}^2$ is a measure of the polydispersity of particle sizes, which ranged from 0.10 to 0.30, indicating a significant size distribution. Average polydispersity values (Table 4) for MIC-CdS1 and MIC-CdS3 (0.29 and 0.28, respectively) were higher than those for MIC-CdS2 and MIC-CdS4 (0.20 and 0.15, respectively). This is consistent with the greater percentage of single chains in MIC-CdS1 and MIC-CdS3 observed by GPC and suggests a lower driving force for chain aggregation for the two samples with protonated PAA layers.

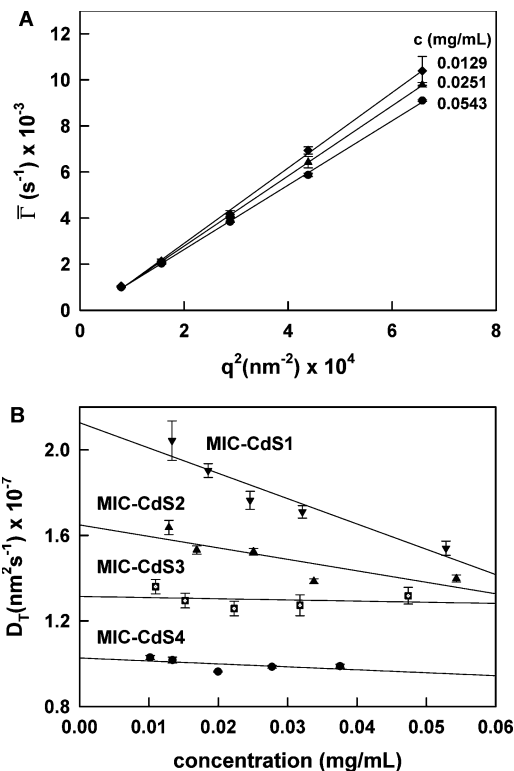


Figure 10. Dynamic light scattering data for the four samples of PS-*b*-PAA-stabilized CdS QDs in toluene. Representative plots of $\bar{\Gamma}$ vs q^2 for various concentrations of MIC-CdS2 in toluene (A) and plots of effective diffusion coefficient D_T vs concentration for the four samples (B).

For all samples and at all concentrations, $\bar{\Gamma}$ was found to scale linearly with q^2 , indicating a diffusive relaxation mode from the free translational diffusion of particles. Representative plots of $\bar{\Gamma}$ vs q^2 for MIC-CdS2 at various concentrations in toluene are shown in Figure 10A. Figure 10B shows plots of effective diffusion coefficients D_T as a function of concentration for each sample and the resulting linear extrapolations to infinite dilution; all of these plots show small negative values of k_d (Table 4), consistent with previous studies of PS-based block ionomer micelles in organic solvents.^{65,67} The hydrodynamic radii r_h of the four samples in toluene (Table 4) range from 18 nm for MIC-CdS1 to 37 nm for MIC-CdS4, increasing with each subsequent treatment of the PAA layer. This range of sizes agrees with previous DLS measurements of block ionomer micelles with PS coronal blocks ~300 units in length,⁶⁷ suggesting that these polymer-coated QDs exist as nonaggregated “brush-like” particles in toluene. The hydrodynamic radius of a spherical polymer brush in a good solvent is known to increase with Z , due to steric-induced chain stretching within the brush. The increases in r_h from MIC-CdS1 to MIC-CdS2 and from MIC-CdS3 to MIC-CdS4 (Table 4) can therefore be understood in terms of increases in aggregation number with Cd²⁺-neutralization of the PAA layer, as observed by GPC in THF solution. The increase in r_h from MIC-CdS2 to MIC-CdS3, however, requires more speculation since GPC results show that the aggregation number of MIC-CdS3 is a factor of 5 lower in THF solution than in MIC-CdS2. Part of this apparent discrepancy in r_h may be related to the increase in size of the encapsulated CdS QD between MIC-CdS2 and MIC-CdS3: subsequent rearrangement of chains with dispersion in toluene may result in

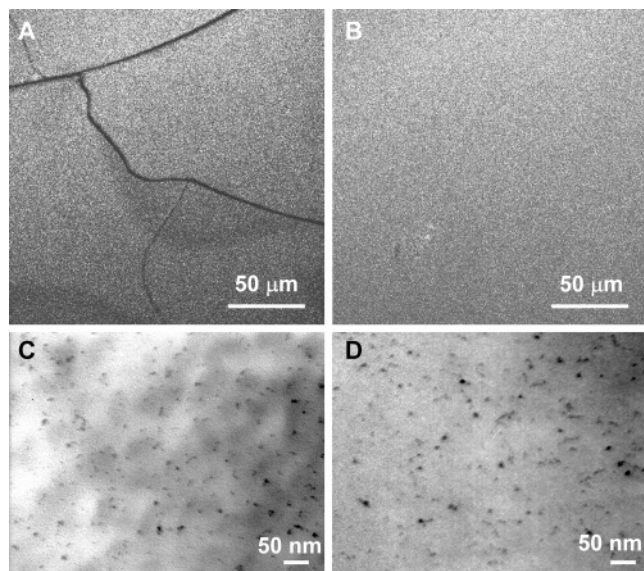


Figure 11. Laser scanning confocal fluorescence microscopy (LSCFM) images of films of 20:80 w/w MIC-CdS4/PS(100) (A) and 20:80 w/w MIC-CdS4/PS(1250) (B). Transmission electron microscopy (TEM) images of films of 20:80 w/w MIC-CdS4/PS(100) (C) and 20:80 w/w MIC-CdS4/PS(1250) (D).

nonuniform packing of copolymer on the surface of the larger QD, such that chain stretching increases despite a lowering of the aggregation number.

QD/PS Homopolymer Blend Films. To demonstrate their effectiveness as dispersible building blocks in polymeric environments, the PS-*b*-PAA-stabilized QDs were solution-blended with PS homopolymer then cast onto glass substrates to obtain optically transparent photoluminescent films. Twenty weight percent of the polymer-coated QDs MIC-CdS4 was blended with 80 wt% of either a high- or low-molecular-weight PS homopolymer (PS(1250) and PS(100), respectively). Both of the resulting blend films had good mechanical properties, although the film containing the low-molecular-weight PS showed a number of cracks following evaporation of solvent. Both blends could be peeled from the glass substrates to produce free-standing films.

Laser scanning confocal fluorescence microscopy (LSCFM) images of the QD blend films prepared using PS(100) (Figure 11A) and PS(1250) (Figure 11B) both showed uniform photoluminescence throughout the ca. 25 μm thick films with 488 nm excitation, indicating that the CdS QDs showed no discernible phase separation from PS(100) or PS(1250) on optical length scales. The dark lines observed in Figure 11A are cracks in the film formed during solvent evaporation. No such cracks were observed in the QD blend film containing the higher-molecular-weight homopolymer PS(1250). TEM images (Figure 11C and D) provide a higher-resolution picture of the structure of these films, revealing excellent dispersion of CdS QDs throughout the PS matrix in both cases, with no observed agglomeration of nanoparticles. LSCFM and TEM images were also obtained after annealing the films at 115 $^{\circ}\text{C}$, above the T_g of PS (~ 100 $^{\circ}\text{C}$), for 8 days; the results in both cases were identical to those before annealing. Clearly, the PS brush layer of the PS-*b*-PAA-stabilized QDs provides favorable interactions with both the PS(100) and the PS(1250) homopolymer, such that the films are thermodynamically stable “solid solutions” of QDs in a polymer “solvent”.

Photoluminescence emission spectra obtained for the QD blend films were nearly identical to that of the MIC-

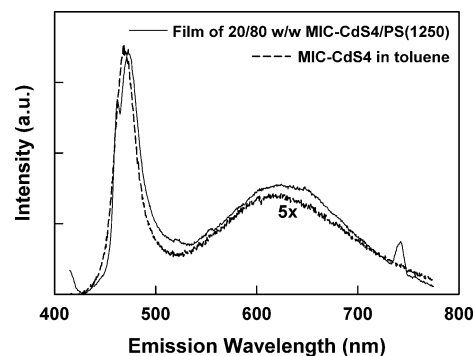


Figure 12. Comparison of photoluminescence emission ($\lambda_{\text{ex}} = 400$ nm) from MIC-CdS4 dispersed in toluene and a film of 20:80 w/w MIC-CdS4/PS(1250).

CdS4 colloidal building blocks dispersed in toluene. Figure 12 compares the emission spectra of the MIC-CdS4/PS(1250) film with that of a dilute toluene solution of MIC-CdS4, revealing that the position and shape of the QD band-edge and trap-state emission are the same in both environments. The nearly identical emission spectra in Figure 12 indicate that no significant increase in particle size has occurred through solution casting and film formation. As well, these results demonstrate that the PAA layer of the block copolymer, along with providing a route to chemically tuning the QD photoluminescence, also maintains a constant surface environment for the QDs while the PS brush layer is dispersed in different environments, such that the nature of surface trap states are the same both in dilute toluene solutions and in polymer blend films. We note that the constant QD surface environment is a function of the high interfacial tension between the PACd layer and the nonpolar external environment of the PS brush layer, which will exclude solvent molecules from interacting with the QD surface, even as the PS brush is solubilized in different media.

Conclusions

This paper describes the first study of static and time-resolved photoluminescence from PS-*b*-PAA-stabilized CdS QDs, demonstrating surface-tunable photoluminescence via chemical treatment of the PAA layer at the surface of the QD. When the PAA layer is in its protonated form, only broad trap-state emission was observed, while neutralization of the PAA layer with cadmium acetate resulted in a reversible sharp increase in the band-edge emission and quantum yield. The “switchable” photoluminescence properties are attributed to passivation of SH⁻ trap states at the surface of the QDs by cadmium carboxylate groups in the neutralized PAA layer, which can be reversed by reprotonation of the acid groups. It was also shown that Cd²⁺ activation of photoluminescence does not occur when Mg²⁺ ions are added to similar QD solutions, indicating potential of these block copolymer-stabilized QDs as Cd²⁺-selective sensors. Excellent long-term stability of the photoluminescence was found for PS-*b*-PAA-stabilized QDs dispersed in toluene, with only a 10% loss in photoluminescence for the dispersion MIC-CdS2 over 57 days under ambient conditions. DLS and GPC measurements with LALS detection revealed significant changes in the aggregation numbers and hydrodynamic radii of the colloidal QDs for different treatments of the PAA layer, with higher block copolymer aggregation numbers for QD samples with a Cd²⁺-neutralized PAA layer, attributed to a lower solubility of the PACd blocks

compared with the acid-form PAA blocks. Finally, it was demonstrated that the PS-*b*-PAA-stabilized QDs could be well dispersed in a matrix of PS homopolymer, producing photoluminescent films which retained the emission features of the constituent colloidal QDs.

This combination of surface-tunable optical properties, provided by the PAA layer, and solubility and stability in polymer and organic media, provided by the PS layer, make PS-*b*-PAA-stabilized QDs ideal candidates as building blocks for higher-order hierarchical structures with potential applications in sensors, biological imaging, and photonic devices. A number of bottom-up approaches to the self-assembly of these unique colloidal QDs in various

environments and on different length scales are currently being explored in our laboratory.

Acknowledgment. The authors gratefully acknowledge the National Science and Engineering Research Council (NSERC), the Canadian Foundation for Innovation (CFI), and the British Columbia Knowledge Development Fund (BCKDF) for their generous support of the research. We also thank Dr. Frank van Veggel and co-workers for their assistance with photoluminescence measurements and Dr. Cornelia Bohne for helpful discussions.

LA048390G